

Modular Multilevel Matrix Converter as Solid State Transformer for Medium and High Voltage AC Substations

Pablo Bravo, *Member, IEEE*, Javier Pereda, *Member, IEEE*, Michael M. C. Merlin, *Member, IEEE*, Sebastian Neira, *Student Member, IEEE*, Timothy C. Green, *Senior Member, IEEE* and Félix Rojas, *Member, IEEE*

Abstract—The use of power converters as solid state transformers is an attractive solution to modernize the power network, but this solution has not been fully addressed for MV and HV substations. This paper presents a customized and simple control for the Modular Multilevel Matrix Converter (M3C), specially conceived for its operation on synchronous ports, which is the case of AC substations. The control allows bidirectional power transfer, generation/absorption of reactive power and provisions of ancillary services. The converter is compared to the back-to-back Modular Multilevel Converter (B2B-MMC) where the key performance indicators to carry out the comparison are power efficiency, number of semiconductor devices, passive components required, footprint, voltage cell balance, fault blocking capability and stress of components. The simulation results show the features, performance and attractiveness of the M3C topology in a 33/11 kV, 16 MW substation under different operating conditions, including grid faults and dynamic operation. The M3C presents similar efficiency and performance than the B2B-MMC, but it uses fewer semiconductor devices, passive components and total cell capacitor energy than the B2B-MMC, reducing cost and footprint. The experimental results show the performance of the M3C under less ideal conditions including a substation transformer saturation and power step response.

Index Terms—Modular multilevel matrix converter, solid state transformer, AC-AC power conversion, power distribution, smart substation, smart grid.

I. INTRODUCTION

INCREASING penetration of variable renewable energies can be detrimental to the transmission and distribution system, leading to alteration of voltage magnitudes such as overvoltage at transmission level buses, greater voltage dips following most of the disturbances and increment of oscillations [1]. The emergence of distributed generation (DG) also introduces significant drawbacks such as power loss increase

The authors acknowledge the support provided by ANID/PIA/ACT192013, ANID/FONDECYT/1220928, ANID/FONDAP/15110019 (SERC Chile) and ESPRC Grant EP/K036327/1.

P. Bravo is with the Department of Electrical Engineering, Pontificia Universidad Católica de Chile, Santiago, Chile. (e-mail: ppbravo@uc.cl).

J. Pereda and F. Rojas are with the Department of Electrical Engineering and the UC Energy Research Center, Pontificia Universidad Católica de Chile, Santiago 7820436, Chile (e-mail: jepereda@ing.puc.cl).

M.M.C Merlin is with the School of Engineering, Institute for Energy Systems, University of Edinburgh, Edinburgh, U.K. (e-mail: Michael.Merlin@ed.ac.uk).

S. Neira is with the Department of Electrical Engineering, Pontificia Universidad Católica de Chile, Santiago, Chile and the School of Engineering, University of Edinburgh, Edinburgh, U.K. (e-mail: sneira@uc.cl).

T. C. Green is with the Department of Electrical and Electronics Engineering, Imperial College, London, U.K. (e-mail: t.green@ic.ac.uk).

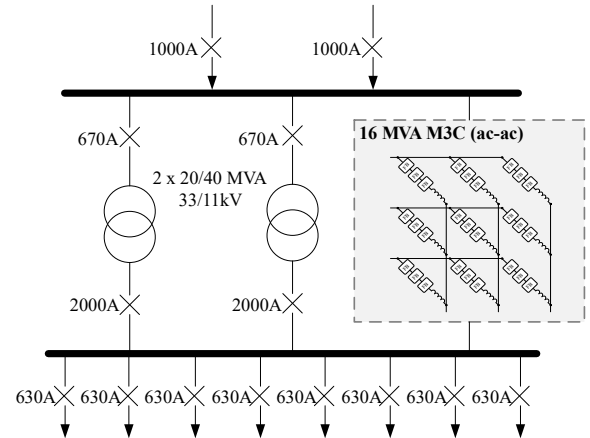


Fig. 1. Modular multilevel matrix converter in MV distribution substation

[2] and poor voltage regulation in the distribution network [3]. A high penetration of EV could generate operational issues in the distribution network [4], which could increase power losses drastically and could require network reinforcements up to 19% [5], especially in urban areas with high load density. The uncoordinated EV charging not only overloads the distribution transformers, but also causes voltage fluctuations and unbalances [6]. The MV network is particularly affected and its transformers need to be resized or upgraded [7].

The traditional solutions such as using taps to control the voltage profile in distribution transformers are not effective in systems with variability, due to high penetration of renewable energies, DG and EVs. Novel solutions have been emerging to overcome this issues. For example, the operation of parallel transformers with different tap positions can provide reactive power absorption services for transmission lines with low demand, which is more economic than using shunt reactors because it uses existing assets, but also increases power losses and introduces voltage spikes [8]. The implementation of intelligent transformer substations in MV networks with remote control and active load management has been proposed to reduce network losses, compensate reactive power, reduce harmonics and monitor the transformer operation during overload [9].

A possible solution is the Solid State Transformer (SST), which is a power electronics interface between MV and LV systems that uses a high frequency transformer. SST is

considered as a key component of the future smart grid and has been widely proposed for distribution networks due to its high controllability and performance, since it has full-range control over voltages and currents. However, for MVA ranges, it is at least five times more expensive and at least three times less efficient than conventional low frequency transformers employed in the grid today [10]. Other important drawbacks are the reliability, operational costs and incompatibility with the protection currently used. Moreover, the application of SST in MV and HV is not straightforward and requires input-series-output-parallel (ISOP) configuration.

On the other hand, Modular Multilevel Converter topologies have been proposed for MV and HV applications such as HVDC transmission, fractional frequency transmission systems [11], [12] and MV motor drives since they have high modularity, reliability and efficiency [13]. The use of MMC in distribution networks is scarce and implemented as B2B-MMC to connect feeders of the same voltage [14] or as hexverter in direct ac-ac configuration [15]. Both converters are promising and can deal with faults and unbalance voltages. However, the use of M3C for distribution networks connecting two synchronous ports has not been addressed, which can be seen as a specific case, but probably the most common case for solid state transformer applications.

This paper presents the M3C (direct ac-ac) applied in HV and MV substations to transfer bidirectional active power, generate or absorb reactive power, provide ancillary services and compares it with the B2B-MMC (indirect ac-dc-ac). The M3C working as solid state transformer in an ac substation can operate under a more simple control scheme than the proposed in previous papers [16]–[18].

II. MODULAR MULTILEVEL TOPOLOGIES

For the use on three phase ac to ac conversion, the Modular Multilevel topologies that stand out are the B2B-MMC, the M3C and the Hex-converter, but the latter is restricted by coupled reactive power between the ac sides [15], therefore, only the first two are further analyzed and compared.

The number of semiconductor devices on the M3C (Fig. 2) is determined by both, the high-voltage (HV) and low-voltage (LV) side voltages, as each stack has to be able to block the maximum possible difference between them to withstand the worst ac fault case scenario. Thus, the minimum number of semiconductor devices (N_{M3C}) on all the full-bridge cells is given by (1), where $\lceil \cdot \rceil$ is the ceiling function, V_{HV}^{rms} and V_{LV}^{rms} are the rms value of the phase to phase voltages at the HV and LV side, respectively, and V_c^{nom} is the nominal value of the cell capacitor voltage.

On the other hand, the number of semiconductor devices on the B2B-MMC (Fig. 3) is determined by the voltage of the HV feeder only, because its magnitude fixes the minimum voltage of the dc-link, which is the voltage that each stack has to be able to block to withstand the worst ac fault case scenario. In this way, the minimum number of semiconductor devices ($N_{B2B-MMC}$) used by all the half-bridge cells is given by (2).

The stacks handle different levels of current, not only between the two converters, but also in the stacks of the

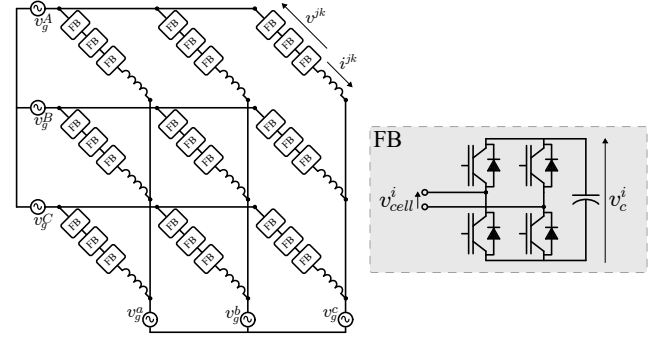


Fig. 2. Topology of a M3C with Full-Bridge (FB) cells.

same converter. For example, considering an operation with the same reactive power in both sides, the B2B-MMC requires controlling a lower current on the HV side. In the case of the M3C, some stacks handle much less current than others, since they depend on the phases to which they are connected and the phase shift of the substation. In this sense, it was decided to preserve the modularity of the converters and operate with IGBTs that support the highest voltages and currents, since in any case the symmetry of the currents in each stack will be reflected in the losses of each converter and in its ability to handle reactive power of greater magnitude.

For the same voltage V_c^{nom} , the ratio between the number of semiconductors in both converters is given by (3), where $\alpha = V_{HV}^{rms}/V_{LV}^{rms}$ and it shows how the higher the voltage ratio, the more disadvantageous the B2B-MMC becomes, as the dc-link forces the LV-MMC to have the same number of semiconductors as the HV-MMC (Fig. 4). For a voltage ratio of $\alpha = 3$, the number of semiconductors used by both converter is the same.

The following comparison of the topologies assumes the same cell capacitor voltages (1.8 kV), same power ratings, same IGBTs and a modular design to block ac faults: in a 33/11 kV substation, the M3C blocks 66% of voltage and has half of capacitors than the B2B-MMC, but both topologies use the same number of IGBTs (720). On the other hand, in a 132/11 kV substation, the M3C blocks 54% of the voltage, has 41% of capacitors and 81% number of IGBTs compared with the B2B-MMC. In summary, the comparison between the two topologies is highly sensitive to the substation voltage ratio with the M3C becoming more attractive at higher voltage ratios. Therefore, the following analysis and comparison are done for a substation with $\alpha = 3$ because it is the most equitable case.

$$N_{M3C} = 4 \cdot 9 \cdot \left\lceil \frac{\sqrt{2} \cdot (V_{HV}^{rms} + V_{LV}^{rms})}{\sqrt{3} \cdot V_c^{nom}} \right\rceil \quad (1)$$

$$N_{B2B-MMC} = 2 \cdot 12 \cdot \left\lceil \frac{2 \cdot \sqrt{2} \cdot V_{HV}^{rms}}{\sqrt{3} \cdot V_c^{nom}} \right\rceil \quad (2)$$

$$\frac{N_{B2B-MMC}}{N_{M3C}} = \frac{4}{3} \cdot \left(\frac{V_{HV}^{rms}}{V_{HV}^{rms} + V_{LV}^{rms}} \right) = \frac{4}{3} \cdot \left(\frac{\alpha}{\alpha + 1} \right) \quad (3)$$

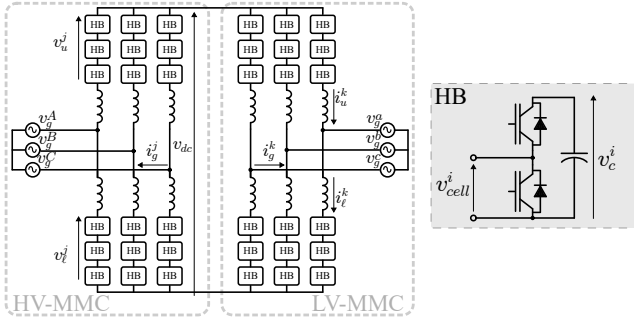


Fig. 3. Topology of a B2B-MMC with Half-Bridge (HB) cells.

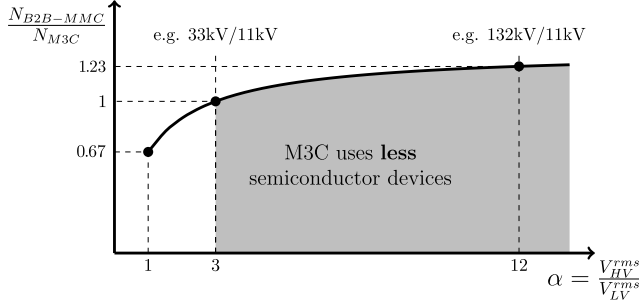


Fig. 4. In terms of the number of semiconductors, the M3C becomes more advantageous than the B2B-MMC for $\alpha > 3$.

III. CONTROL OF THE MMC CONVERTERS

For an adequate comparison, the control schemes used for the B2B-MMC and the M3C share the same structure. A current solver with the model equations of each topology controls the active and reactive power on both sides of the substation. Then, cascaded PI and P+R controllers regulate the arm currents and balance the energy between stacks. Finally, phase-shift PWM is implemented with a proportional controller to balance the voltage of the cell capacitors within each stack. The following subsections explain each control in detail.

A. Control of the back-to-back MMC

The control scheme for the B2B-MMC uses three outer PI energy controllers to balance the energy between the stacks plus two inner current controllers per leg (Fig. 6).

The horizontal controller (P_h) receives the energy stored in the upper and lower stack capacitors, and it regulates this value so that the stored energy in the leg matches the set point. On the other side, the vertical controller (P_v) takes the difference between the energy of the upper and lower stack, and regulates its value to zero to keep the same energy on both stacks. The third controller (P_{dc}) regulates the dc-link voltage to match the reference value. The dc-link exchanges energy with the LV and/or HV side of the grid according to a fixed scalar $k_e \in [0, 1]$ set by the operator.

The currents of the upper and lower arm of the same leg j , are used in the following linear transformation $T_{\Sigma\Delta}$ [19], [20] to decouple the model:

$$\begin{bmatrix} i_{out}^j \\ i_{circ}^j \end{bmatrix} = \begin{bmatrix} 1 & -1 \\ \frac{1}{2} & \frac{1}{2} \end{bmatrix} \begin{bmatrix} i_u^j \\ i_l^j \end{bmatrix}, \quad j \in \{A, B, C, a, b, c\} \quad (4)$$

The output current i_{out} regulates the active and reactive power at both sides of the substation, and the circulating current i_{circ} regulates the power given by the outer PI controllers to balance the capacitors.

The model equations of the current solver that calculates the current references for each phase j are given in (5) and (6), using the power variables defined in (7) and (8).

$$i_{out}^j = \frac{P^j - jQ^j}{v^j} \quad (5)$$

$$i_{circ}^j = \frac{P^j + P_h^j + P_v^j}{v_{dc}} \quad (6)$$

$$P^j = \frac{-P^* - k_e P_{dc}}{3}, \quad Q^j = \frac{Q_{HV}^*}{3}, \quad j \in \{A, B, C\} \quad (7)$$

$$P^j = \frac{P^* - (1 - k_e) P_{dc}}{3}, \quad Q^j = \frac{Q_{LV}^*}{3}, \quad j \in \{a, b, c\} \quad (8)$$

B. Proposed control of the M3C

The control scheme used for the M3C has one outer PI energy controller per arm for the stored energy in each stack and one inner P+R current controller per arm (Fig. 7).

The outer PI power controller regulates the energy of each stack E_s^{jk} through injection or absorption of active power P_s^{jk} . Ideally, the cell capacitors do not exchange active power, so only a quadrature current should flow through each arm, but P_s^{jk} is injected or absorbed in case of unbalances.

The current solver calculates the reference current for each arm i^{jk} through the model equations (9)-(12). The solver receives the power references of each grid line from a tertiary control (grid operator or high-level control) and it receives the active power P_s^{jk} of each stack from the outer PI controller.

The line currents i^j at HV and LV sides are defined by the power reference from the tertiary control (grid operator or high-level control). Additionally, each line current is the sum of the three arm currents connected to the respective line, so they can be expressed by a matrix equation system (9), but matrix M is rank deficient, hence the arm currents cannot be obtained directly. On the other hand, the arm current i^{jk} can be split into direct (or x) i_x^{jk} and quadrature (or y) i_y^{jk} components as illustrated in Fig. 5, which are related to the real and imaginary components by the rotation matrix (10).

The power P_s^{jk} defines the active current of the respective arm i_x^{jk} (12), where v^{jk} is the difference of the respective phase voltages (13), and the arm voltage angle θ^{jk} is used as reference for the real axis of the arm currents i_{xy}^{jk} . Equation (11) is solved for i_y and the arm currents i^{jk} are obtained from the linear transformation (10) as the system becomes fully ranked.

$$M \cdot \begin{bmatrix} \Re(i^{Aa}) \\ \Im(i^{Aa}) \\ \vdots \\ \Re(i^{Cc}) \\ \Im(i^{Cc}) \end{bmatrix} = \begin{bmatrix} \Re(i^A) \\ \Im(i^A) \\ \vdots \\ \Re(i^c) \\ \Im(i^c) \end{bmatrix} = i^\ell, \quad M \in \mathbb{R}^{12 \times 18} \quad (9)$$

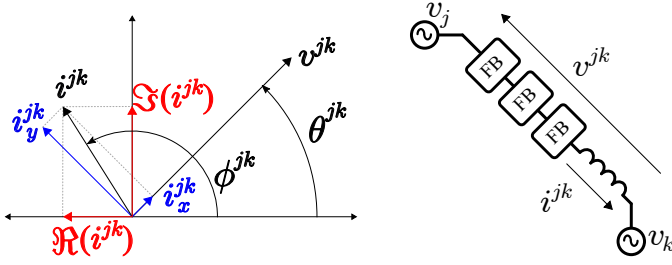


Fig. 5. Current coordinates for M3C modelling.

$$\begin{bmatrix} \Re(i^{jk}) \\ \Im(i^{jk}) \end{bmatrix} = \begin{bmatrix} \cos(\theta^{jk}) \\ \sin(\theta^{jk}) \end{bmatrix} \begin{bmatrix} i_x^{jk} \\ i_y^{jk} \end{bmatrix} + \begin{bmatrix} -\sin(\theta^{jk}) \\ \cos(\theta^{jk}) \end{bmatrix} \begin{bmatrix} i_x^{jk} \\ i_y^{jk} \end{bmatrix} \quad (10)$$

$$M_x \cdot i_x + M_y \cdot i_y = i^\ell \quad (11)$$

$$S^{jk} = (|v^{jk}| \cdot i_x^{jk}) - j(|v^{jk}| \cdot i_y^{jk}) \Rightarrow i_x^{jk} = \frac{P_s^{jk}}{|v^{jk}|} \quad (12)$$

$$|v^{jk}| \angle \theta^{jk} = v^j - v^k, j \in \{A, B, C\}, k \in \{a, b, c\} \quad (13)$$

IV. SIMULATION RESULTS

The converter was simulated in a 33kV/11kV, 16 MVA substation with a Dy1 configuration ($\Delta\theta = 30^\circ$) because it is common for MV distribution transformers [21]. The voltages 33/11 kV were chosen because it is the most equitable case for the comparison of both topologies, according to section II. The simulations were computed using MATLAB/Simulink SimPowerSystems toolbox using the key parameters of the power system summarized in Table I.

Table II indicates the parameters of the simulated M3C and also of its B2B-MMC counterpart. The number of cells and their capacitance value were selected to handle 16 MVA with a maximum voltage ripple of $\pm 10\%$ in each capacitor. The capacitance of the cells was sized using a standard approach [22] to handle a maximum desired voltage ripple ($\pm 10\%$) on each converter at the worst case scenario, which is the operating point that generates the most ripple. For the B2B-MMC, the calculation is straightforward with the HV side MMC requiring $1/\alpha$ of capacitance needed in the LV side. On the other hand, the capacitor sizing for the M3C was obtained by a numerical method via iteration algorithms. The capacitance is highly dependant on the voltage ratio α and on the phase angle δ between both sides of the substation. The same inductors were used in both converters to maintain fairness in the harmonic distortion comparison. The same switching frequency of the cells was selected for both converters to maintain fairness in the THD and efficiency comparison. The PS-PWM works at 200 Hz because it exhibits a good trade-off between switching power losses and current THD. Both converters are transformerless and filterless to reduce cost, footprint and power losses. They can be connected directly to the MV grid because they manage high voltage and generate a great number of voltage levels in each stack (31 for B2B-MMC and 41 for M3C). The gains of the current and energy controllers were tuned heuristically to achieve relatively fast

response without an excessive overshoot. The converter has a maximum reactive power in the HV grid side three times higher than in the LV side, since each arm was sized to handle the LV side current.

The following subsections show the operation of the converter under different scenarios. First, the power losses and efficiencies are calculated for various stationary power operating points and compared to the B2B-MMC efficiencies at same conditions. Then, key waveforms are presented to observe the performance under four situations: (i) nominal power transmission and ideal conditions; (ii) dynamic power flow operation; and (iii) single-phase to ground and three-phase to ground short circuit faults.

A. Power Losses

The power losses in the semiconductor devices were obtained by using the curves of the ABB IGBT part 5SNA1200E330100 (3.3 kV, 1.2 kA) provided by the manufacturer and according to the standard BS EN 62751:2014 [23], [24]. The following power losses were considered: (i) IGBT conduction losses; (ii) IGBT turn-on and (iii) turn-off switching losses; (iv) diode reverse recovery losses; and (v) diode conduction losses. The losses in the arm reactors due to its equivalent series resistance were also calculated and added to the efficiency results because they can represent up to 10% of the total losses. Other power losses such as additional conduction losses, capacitor losses and driver power consumption, were not taken into account as they are comparatively negligible and there is no need for snubber circuits [25].

Table III shows the efficiency of the converters for several power flow operating points. The efficiency of the B2B-MMC and M3C at nominal power and unity power factor is 97.79% and 97.41%, respectively. As the power decreases, the switching losses becomes more relevant than the conduction losses, while the total power losses do not follow a direct relationship. Also, losses remain similar when the power reverse. The converters present lower efficiencies when operating at nominal power with low power factors, particularly when it is at the high-voltage side.

The B2B-MMC shows higher efficiency than the M3C at unity power factor, regardless of the amount of power being transferred. On the other hand, the M3C shows better efficiency than the B2B-MMC when considerable amount of reactive power is injected at the HV side. Both converters exhibit the same efficiency when they are operated at nominal power with a power factor angle of 45° on the LV side.

TABLE I
PARAMETERS OF THE SYSTEM

Description	Parameter	Value
Grid nominal frequency	f	50Hz
HV Grid nominal voltage	V_{HV}^{l-l}	33kV $\angle 30^\circ$
LV Grid nominal voltage	V_{LV}^{l-l}	11kV $\angle 0^\circ$
HV Grid X/R	$X R_{HV}$	10
LV Grid X/R	$X R_{LV}$	30
Short circuit level	S_{sc}	500MVA

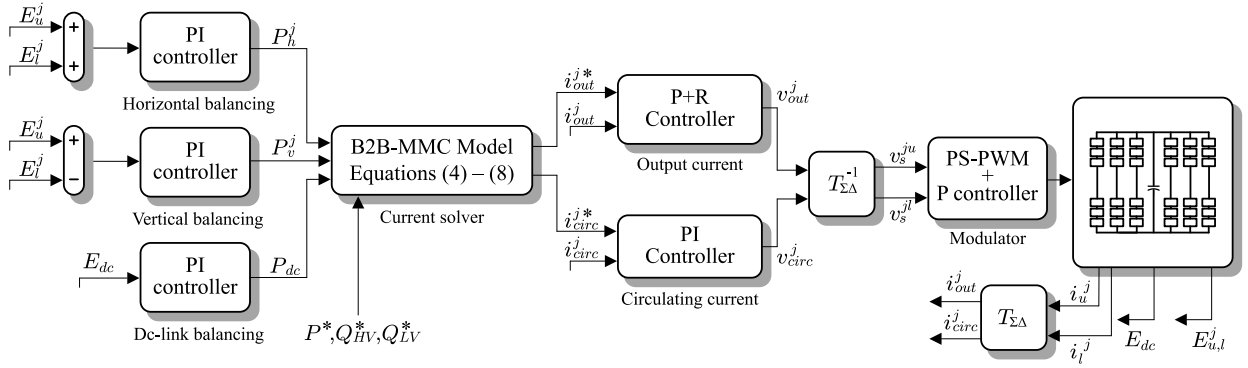


Fig. 6. Control scheme for the B2B-MMC.

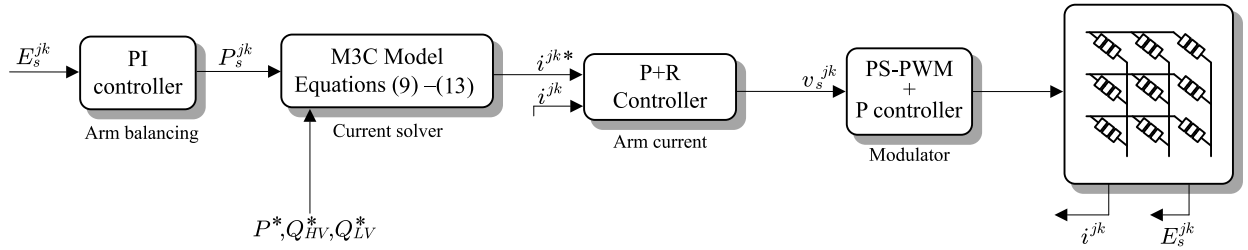


Fig. 7. Control scheme for the M3C.

TABLE II
PARAMETERS OF THE CONVERTERS ($V_{base}^{l-l} = 11 \text{ kV}$)

Description	Parameter	Value	
		B2B-MMC	M3C
Power rating	S_{nom}	16 MVA	
Arm reactor inductance	L	4.8 mH (0.2 pu)	
Arm reactor resistance	r_L	15.8 m Ω (Q=100)	
Switching frequency	f_s	200 Hz	
IGBT 5SNA1200E330100	—	3.3 kV & 1.2 kA	
Cell capacitors voltage	V_C	1.8 kV	
Cell capacitors size	C	1.75 mF (HV) 5.25 mF (LV)	3.27 mF
Cells per arm	N	30	20
Number of cells	N_t	360	180
Number of IGBTs	N_{igbt}	720	720
Number of voltage sensors	N_{vs}	360	180
Number of current sensors	N_{cs}	12	9
Total cell energy	E_{cap}	2041 kJ	954 kJ
Stack switching frequency	f_{sw}	6 kHz	8kHz

TABLE III
EFFICIENCY ($T_{vj} = 25^\circ\text{C}$)

P	Q_{HV}	Q_{LV}	$\eta_{B2B-MMC}$	η_{M3C}
1.0 p.u.	0.0 p.u.	0.0 p.u.	97.79%	97.41%
0.5 p.u.	0.0 p.u.	0.0 p.u.	97.87%	97.59%
0.1 p.u.	0.0 p.u.	0.0 p.u.	97.65%	97.55%
-1.0 p.u.	0.0 p.u.	0.0 p.u.	97.80%	97.54%
$\sqrt{0.5}$ p.u.	0.0 p.u.	$\sqrt{0.5}$ p.u.	97.25%	97.25%
1.0 p.u.	$\sqrt{8.0}$ p.u.	0.0 p.u.	96.91%	97.06%
$\sqrt{0.5}$ p.u.	$\sqrt{8.5}$ p.u.	$\sqrt{0.5}$ p.u.	95.85%	96.69%

B. Performance Under Ideal Conditions

Fig. 8a shows the results for the M3C simulated at nominal operation (16 MVA) and unity power factor with active power flowing from HV to LV side and compares it with Fig. 8b which shows the operation of the B2B-MMC under the same conditions. Both converters exhibit voltages and currents with relatively low THD for the two sides (33 kV and 11 kV). This shows the high power quality of the converters, which could outperform the conventional low frequency transformer, as it is an active system able to control active and reactive power in all four quadrants, control currents independently and filter harmonics. The latter enables the provision of several ancillary services which enhance the power quality of the

system. However, this proposal does not cover the ancillary services and focuses on the power control of the converters as solid state transformer.

The arm currents in the M3C only have an ac component, whereas in the B2B-MMC they also include a dc component whose sign depends on the direction of the active power flow. The stack voltages of the M3C are multilevel sinusoidal waveforms without offset, in contrast to the ones of the B2B-MMC which have an offset equal to half the dc-link voltage.

The cells capacitor voltages are well balanced with a ripple that depends on the operating point and the capacitance of the cells. The B2B-MMC converter capacitors exhibit a grid frequency ripple with an additional second harmonic component that can reach up to 1/4 the magnitude of the fundamental. The capacitance of the cells were selected to keep the ripple constraint at 10% for the worst case scenario, so at this operating point the ripple does not reach its limits.

C. Performance Under Dynamic Power Operation

The performance of the converter was tested under a dynamic power operation over a period of 0.1 seconds. The

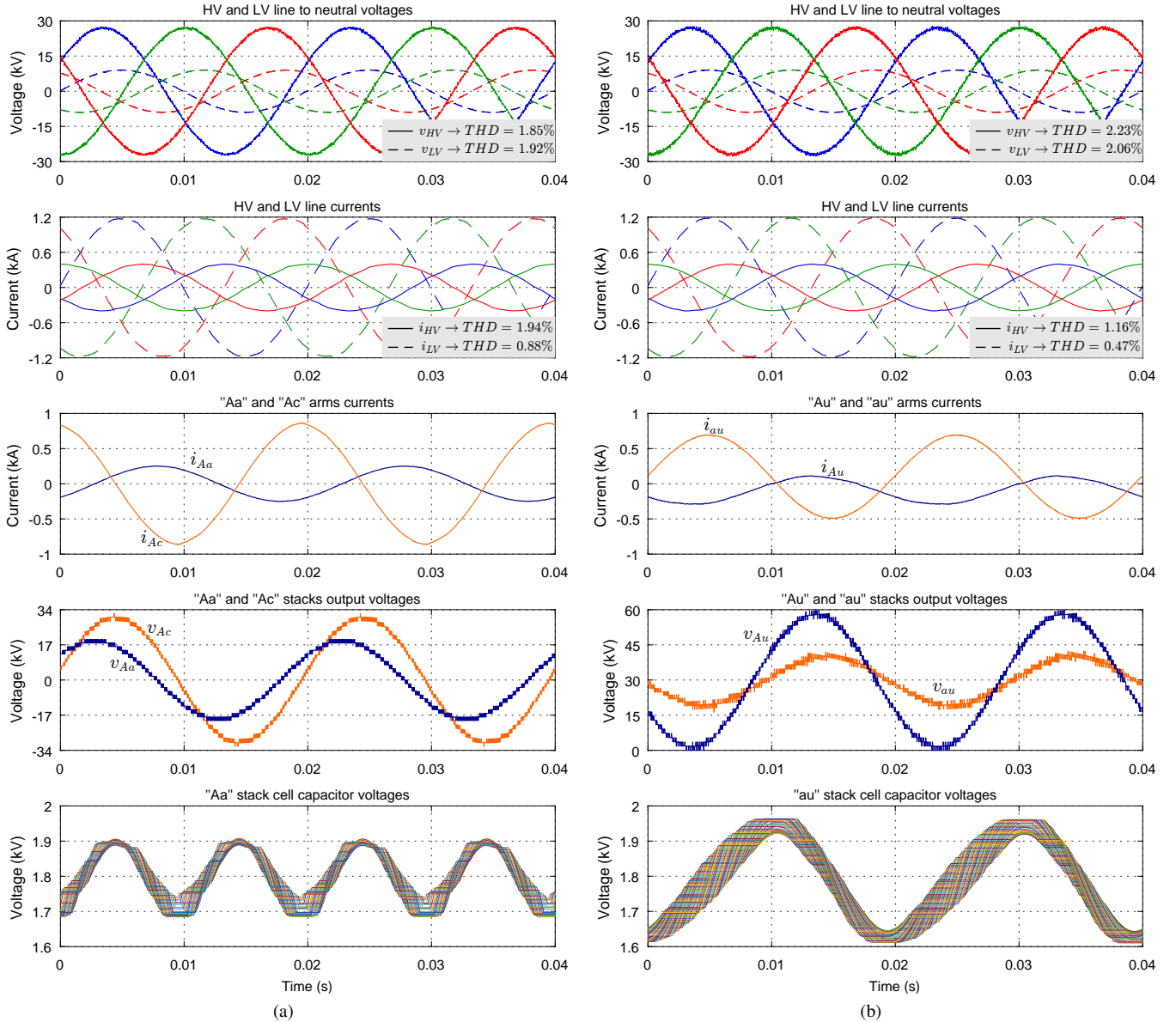


Fig. 8. Waveforms of (a) the M3C and (b) the B2B-MMC under ideal conditions.

operation consists in an active power reversal ($P_{LV} = -P_{HV}$ from 0.7 to -0.7 p.u), a reactive power reversal at LV side (Q_{LV} from 0.5 to -0.5 p.u), and a reactive power drop at HV side (Q_{HV} from 2.8 to 2.0 p.u).

The results of this simulations are shown in Fig. 9. Active and reactive power follow the reference precisely and accurately while the line currents change smoothly during the transition. The moving average of the mean cell capacitor voltage in each stack are maintained near the reference.

The arm current amplitudes are coupled in groups of three ($[i_{Ac}-i_{Ba}-i_{Cb}]$; $[i_{Aa}-i_{Bb}-i_{Cc}]$; $[i_{Ab}-i_{Bc}-i_{Ca}]$) and they control the power by changing their magnitude while maintaining their phase.

D. AC Fault Blocking Capability

The ability to cope with ac fault was tested. The control system detects a fault when the line voltage drops under 60%

of its nominal value. If a fault is detected, the magnitude of the reference of the arm currents is decreased to zero with a rate limiter to avoid peak voltages across the arm reactors. For a complete current stop, the IGBTs were programmed to open as soon as the currents reach zero. When the voltage is restored, the converters resume their normal operation with the appropriate rate limiter.

Fig. 10 shows the results of two simulations that include faults between 0.05s and 0.08s at the LV side of the converters while operating at $P_{LV} = -P_{HV} = 0.3$, $Q_{LV} = 0.1$, and $Q_{HV} = 0.5$. Fig. 10a shows a unsymmetrical single-phase to ground fault and Fig. 10b shows a symmetrical three-phase to ground fault.

The converter can appropriately set to zero the power flow between HV and LV side during the fault and quickly get back to the previous operating point when the fault is cleared. This

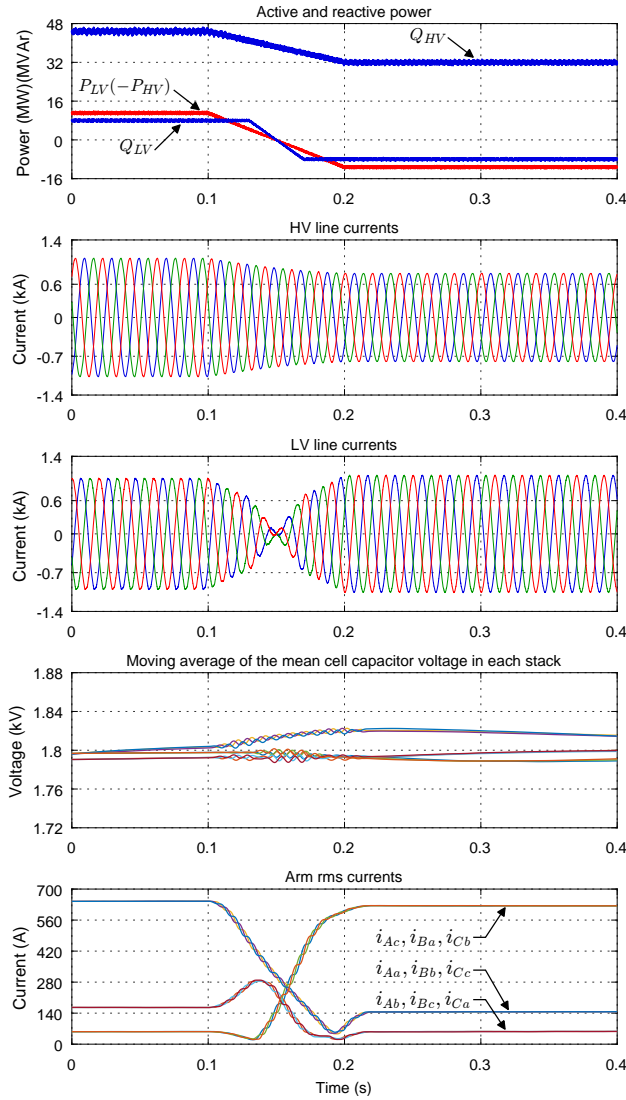


Fig. 9. Waveforms of the M3C under dynamic operation.

is shown as a moving average of the power flow within each phase. For the duration of the fault, the voltage in capacitors remain constant since there is no arm current. When the fault is gone, the energy controllers return to balance the voltage in the capacitors instantaneously.

The presented results demonstrate the ability of the converter to cope with ac faults without needing galvanic isolation, which is the main concern with non-isolated SST [26]. Furthermore, current substations can work using autotransformers [27], which means that a non-isolated converter as the M3C could be a suitable alternative for substations.

V. EXPERIMENTAL RESULTS

An M3C prototype was constructed and tested in a 570V/190V (330V/110V line to neutral) experimental substation. The substation consisted of the three phase Chilean residential grid (380V at 50 Hz) feeding a three-phase 380V/570V dY1 transformer for the HV side and a three-phase autotransformer, which was previously set to an output of 190V, for

TABLE IV
PARAMETERS OF THE ELECTRICAL SYSTEM AND CONVERTER
($V_{base}^{l-l} = 190\text{ V}$)

Description	Parameter	Value
Grid nominal frequency	f	50 Hz
HV Grid nominal voltage	V_{HV}^{l-l}	570 V $\angle -30^\circ$
LV Grid nominal voltage	V_{LV}^{l-l}	190 V $\angle 0^\circ$
Power rating	S_{nom}	5 kVA
Arm reactor inductance	L_{arm}	5.0 mH (0.3 pu)
Arm reactor resistance	R_{arm}	5.0 m Ω (Q=300)
Switching frequency	f_s	1 kHz
MOSFET CoolMOS IPW65R041CFD	–	650 V & 68.5 A
Cell capacitors voltage	V_C	155 V
Cell capacitors size	C	1.00 mF
Cells per stack	N	4
Total number of cells	N_t	36
Total number of IGBTs	N_{igbt}	144
Total cell energy	E_{cap}	432 J
Stack switching frequency	f_{sw}	8 kHz

the LV side. The converter consisted of an M3C with four H-bridge cells and a 5mH inductor per leg. A simple schematic of the setup is shown in Fig. 11.

The parameters of the converter such as number of cells, cell nominal voltage and capacitance were selected following the same procedure as for the simulations, in this case for a nominal power of the converter of 5kVA and a maximum voltage ripple of $\pm 10\%$ in each capacitor, resulting in 4 cells per stack, with a nominal voltage 155V and 1mF capacitance per cell. The parameters of the electrical system and the converter are shown in table IV.

The following sections show the operation of the converter prototype under two different scenarios: (i) steady state operation and (ii) dynamic power flow operation. It was not possible to test the operation of the converter under fault conditions due to the laboratory current protection scheme.

A. Performance under steady state operation

Fig. 12a shows the behaviour of the M3C at steady state operation with an active power flow reference of 0.6 p.u. from HV (570V) to LV (190V) side, a reactive power flow reference of 1.8 p.u. at the HV side and 0.45 at the LV side.

The voltages of the HV and LV grid show a high level of switching frequency harmonic ripple. Due to the low short-circuit level of the setup, the sudden changes of 155V at the output of the cells influence the grid voltage seen by the converter.

The line currents show a much lower switching harmonic ripple, but a considerable presence of low order harmonics, due to the saturation of the transformers when operated above their nominal power which results in a non-linear relationship between voltage and current over certain value. The saturation point is not the same for both sides, because the two transformers are of different types and from different manufacturers.

Arm currents follow the references (in black) accurately with some switching frequency ripple, inherent feature of the multilevel converters with this number of levels and switching frequency. One way of reducing the presence of ripple is

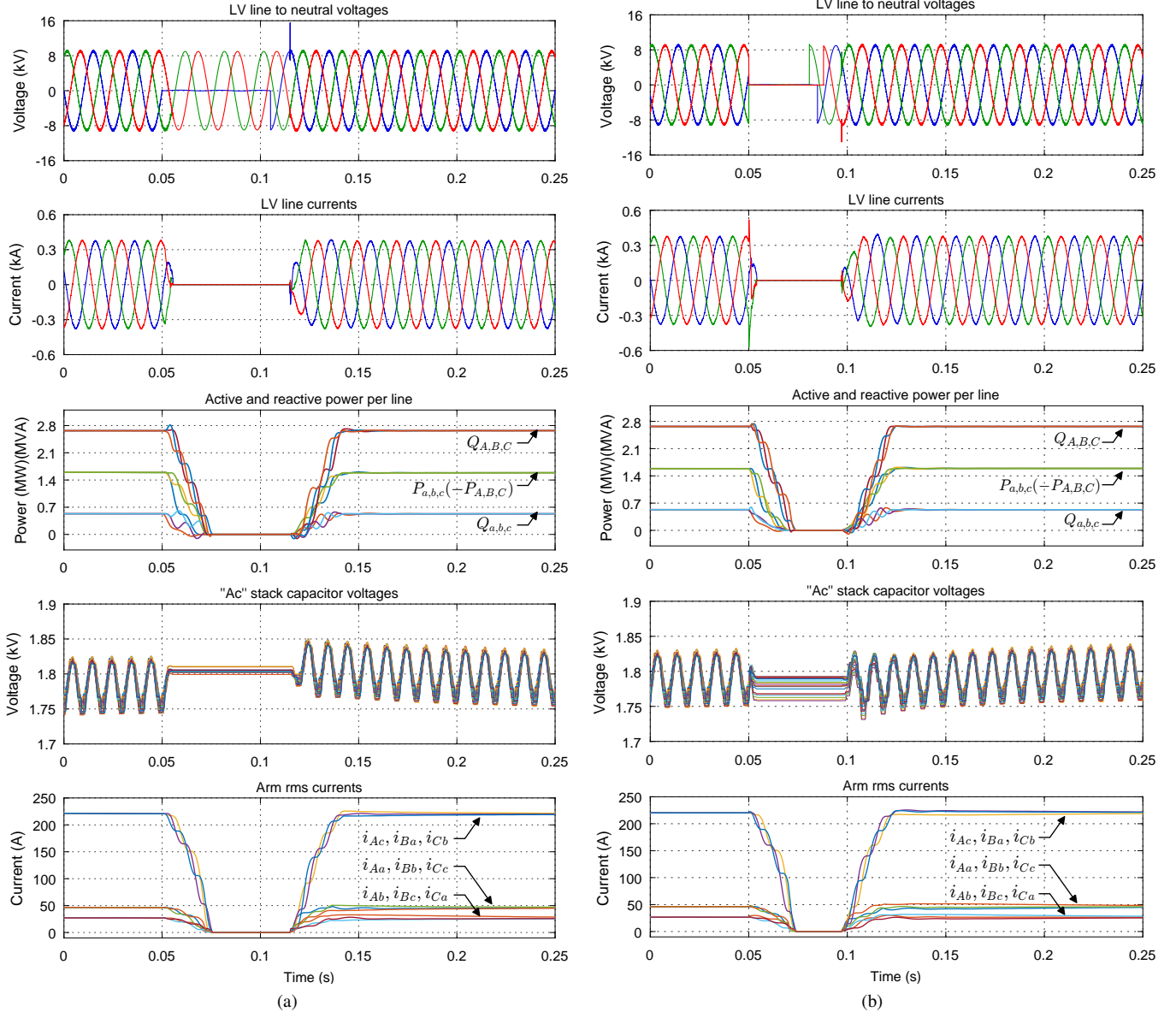


Fig. 10. Waveforms of the M3C under (a) unsymmetrical single-phase to ground fault at LV and (b) symmetrical three-phase to ground fault at LV.

to increase the switching frequency of the stacks, by either increasing the number of levels or increasing the switching frequency of the cells, but the latter increases the switching losses.

The capacitor voltages of the cells are well balanced with the characteristic fundamental component with twice the grid frequency. Since the capacitance of the cells were selected to keep the ripple constraint for the worst case scenario, the ripple is less than 10%. Fig. 12a only shows the capacitor voltages of one arm, but all of them were kept between the ripple limits.

B. Performance under dynamic operation

The performance of the prototype was tested under a dynamic operation with power references ramping to new values over a period of 0.1 seconds. The operation consists of an active power reversal ($P_{LV} = -P_{HV}$ from 0.6 to -0.6 p.u.),

a reactive power reversal at LV side (Q_{LV} from 0.45 to -0.45 p.u.), and a step reactive power drop at HV side (Q_{HV} from 1.8 to 1.3 p.u.).

The results of this test are shown in Fig. 12b. During the dynamic operation the changes are not as smooth as shown by the simulations because, in contrast with the condition of the simulations, the transition time given to the reactive power at the HV side was of 0.01s instead of 0.1s. Nevertheless, active and reactive power are well established into the desired value after the transition and the moving average of the mean cell capacitor voltage in each stack is well controlled to return to the reference of 155V.

VI. CONCLUSION

The M3C has been shown to be suitable for HV and MV ac substations working as grid supporting converters,

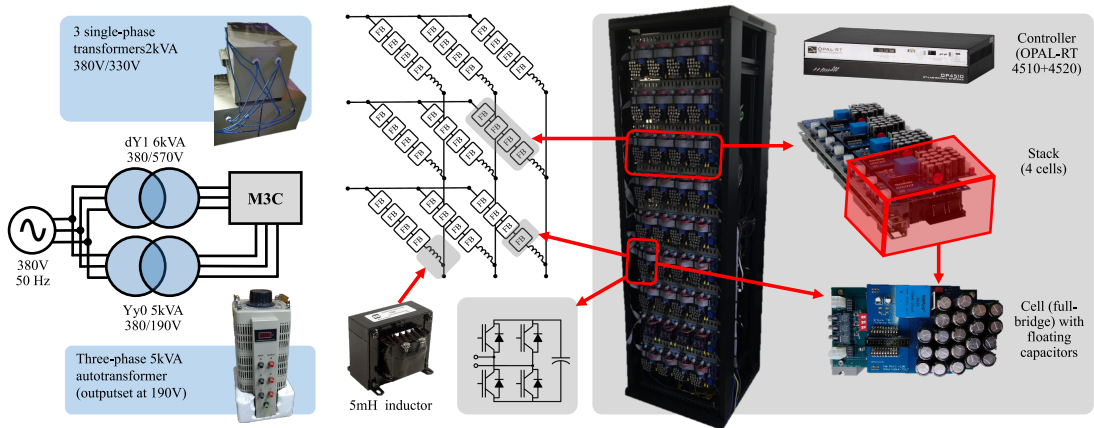


Fig. 11. Experimental setup configuration.

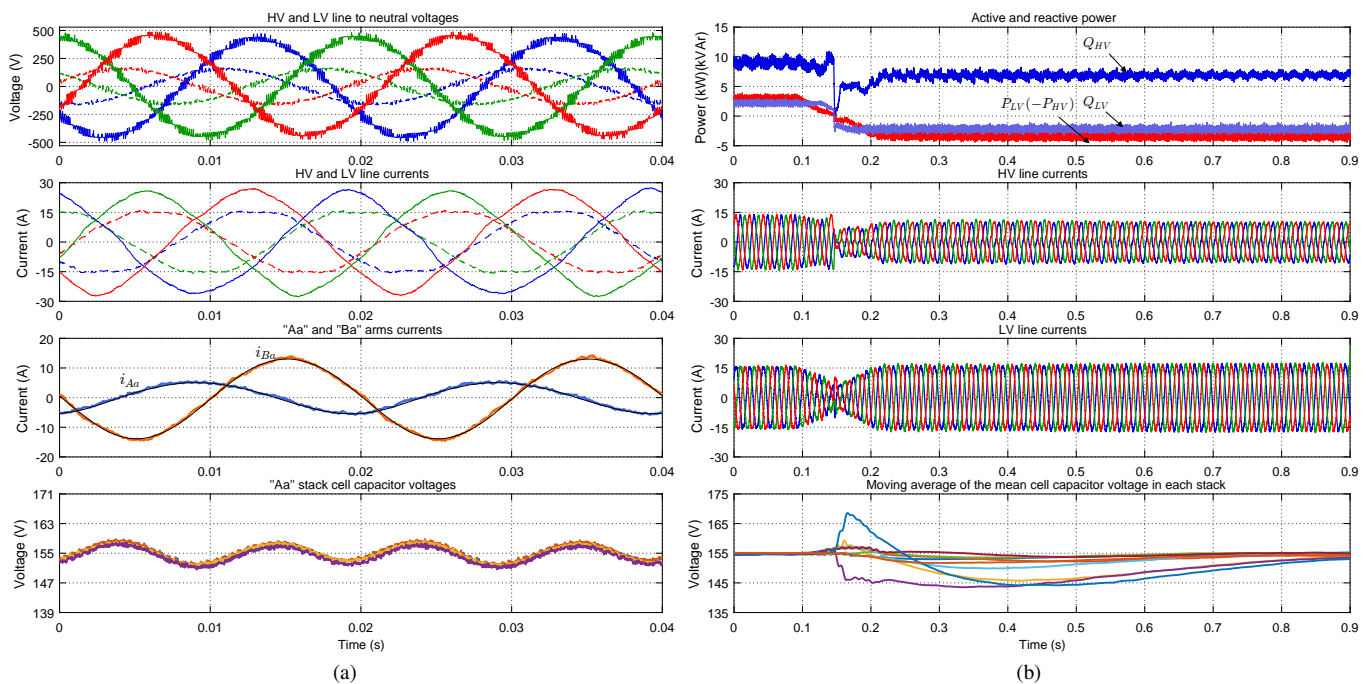


Fig. 12. Waveforms of the M3C experimental setup under (a) steady state and (b) dynamic operation.

connected in parallel with conventional transformers. This power converter combines the benefits of the MMC, such as high modularity, reliability, efficiency and quality waveforms with the benefits of the SST, such as high controllability and performance.

The proposed control of the M3C introduces a new transformation that decouples the output and circulating currents and works under synchronous operation. The control scheme achieves bidirectional active power transfer, decoupled generation and absorption of reactive power at both sides of the converter and ac fault blocking.

Simulations of a 33/11 kV, 16 MVA substation show that the converter can successfully operate under normal conditions achieving low power losses and currents with low THD, dispensing with the use of line filters. Simulations also show quick response of the converters during ac fault events. This

ability of the converter to cope with faults can be extrapolated to other types of faults as the converter can easily stop the current flow by opening the IGBTs, which avoids the need for galvanic isolation in the substation.

Experimental results on a 570/190 kV, 5 kVA prototype substation show that the M3C can operate under steady state and dynamic conditions being able to follow the power references and balancing the capacitor voltages even for step changes in the reference and with saturated transformers.

Compared with the B2B-MMC, the M3C uses half the number of cells and has 47% of the total cell capacitors energy in a 33/11 kV substation. This means the footprint of the capacitors will be significantly reduced in the M3C, which can be a determinant parameter to choose the topology over the B2B-MMC. The M3C becomes even more attractive at higher voltage ratios as it also uses fewer semiconductors. The

high number of semiconductor devices in Modular Multilevel Converters makes them still an expensive alternative to transformers, but it was concluded that the M3C converter should be more economic than the B2B-M2C where the substation has a voltage ratio higher than 3:1. Additionally, in the future it is expected that the ancillary services the M3C can provide will reduce the economic gap, making them a very attractive solution.

The efficiency of the power converter is lower than a conventional transformer, but is high in comparison to solid state transformers [10]. Additionally, this converter could deliver several ancillary services, work as grid forming converters or can be operated with the goal of optimize the efficiency of the entire substation if it is implemented in parallel with conventional transformers, which can be analyzed in a future work.

REFERENCES

- [1] S. Eftekharnjad, V. Vittal, G. T. Heydt, B. Keel, and J. Loehr, "Impact of increased penetration of photovoltaic generation on power systems," *IEEE Transactions on Power Systems*, vol. 28, no. 2, pp. 893–901, May 2013.
- [2] V. H. M. Quezada, J. R. Abbad, and T. G. S. Roman, "Assessment of energy distribution losses for increasing penetration of distributed generation," *IEEE Transactions on Power Systems*, vol. 21, no. 2, pp. 533–540, May 2006.
- [3] P. N. Vovos, A. E. Kiprakis, A. R. Wallace, and G. P. Harrison, "Centralized and Distributed Voltage Control: Impact on Distributed Generation Penetration," *IEEE Transactions on Power Systems*, vol. 22, no. 1, pp. 476–483, Feb 2007.
- [4] P. Richardson, D. Flynn, and A. Keane, "Impact assessment of varying penetrations of electric vehicles on low voltage distribution systems," in *IEEE PES General Meeting*, July 2010, pp. 1–6.
- [5] L. P. Fernandez, T. G. S. Roman, R. Cossent, C. M. Domingo, and P. Frias, "Assessment of the Impact of Plug-in Electric Vehicles on Distribution Networks," *IEEE Transactions on Power Systems*, vol. 26, no. 1, pp. 206–213, Feb 2011.
- [6] P. Maheshwari, Y. Tambawala, H. S. V. S. K. Nunna, and S. Doolla, "A review on plug-in electric vehicles charging: Standards and impact on distribution system," in *2014 IEEE International Conference on Power Electronics, Drives and Energy Systems (PEDES)*, Dec 2014, pp. 1–6.
- [7] Q. Wu, L. Cheng, U. Pineau, A. H. Nielsen, and J. Østergaard, "Impact and cost evaluation of electric vehicle integration on medium voltage distribution networks," in *2013 IEEE PES Asia-Pacific Power and Energy Engineering Conference (APPEEC)*, Dec 2013, pp. 1–5.
- [8] L. Chen, H. Y. Li, S. Cox, and K. Bailey, "Ancillary Service for Transmission Systems by Tap Stagger Operation in Distribution Networks," *IEEE Transactions on Power Delivery*, vol. 31, no. 4, pp. 1701–1709, Aug 2016.
- [9] H. Spack, B. Schupferling, J. Riemenschneider, and M. Schelte, "Intelligent transformer substations in modern medium voltage networks as part of "smart grid"," in *7th Mediterranean Conference and Exhibition on Power Generation, Transmission, Distribution and Energy Conversion (MedPower 2010)*, Nov 2010, pp. 1–7.
- [10] J. E. Huber and J. W. Kolar, "Applicability of Solid-State Transformers in Today's and Future Distribution Grids," *IEEE Transactions on Smart Grid*, pp. 1–1, Aug 2018.
- [11] S. Liu, X. Wang, L. Ning, B. Wang, M. Lu, and C. Shao, "Integrating offshore wind power via fractional frequency transmission system," *IEEE Transactions on Power Delivery*, vol. 32, no. 3, pp. 1253–1261, 2017.
- [12] S. Liu, X. Wang, Y. Meng, P. Sun, H. Luo, and B. Wang, "A decoupled control strategy of modular multilevel matrix converter for fractional frequency transmission system," *IEEE Transactions on Power Delivery*, vol. 32, no. 4, pp. 2111–2121, 2017.
- [13] M. A. Perez, S. Bernet, J. Rodriguez, S. Kouro, and R. Lizana, "Circuit Topologies, Modeling, Control Schemes, and Applications of Modular Multilevel Converters," *IEEE Transactions on Power Electronics*, vol. 30, no. 1, pp. 4–17, Jan 2015.
- [14] M. Chiandone, G. Sulligoi, F. Milano, G. Piccoli, and P. Mania, "Back-to-back MVDC link for distribution system active connection: A network study," in *2014 International Conference on Renewable Energy Research and Application (ICRERA)*, Oct 2014, pp. 1001–1006.
- [15] J. Pereda and T. C. Green, "Direct Modular Multilevel Converter With Six Branches for Flexible Distribution Networks," *IEEE Transactions on Power Delivery*, vol. 31, no. 4, pp. 1728–1737, Aug 2016.
- [16] F. Kammerer, J. Kolb, and M. Braun, "Fully decoupled current control and energy balancing of the modular multilevel matrix converter," in *2012 15th International Power Electronics and Motion Control Conference (EPE/PEMC)*, 2012, pp. LS2a.3–1–LS2a.3–8.
- [17] M. Espinoza, R. Cárdenas, M. Díaz, and J. C. Clare, "An enhanced dq -based vector control system for modular multilevel converters feeding variable-speed drives," *IEEE Transactions on Industrial Electronics*, vol. 64, no. 4, pp. 2620–2630, 2017.
- [18] B. Fan, K. Wang, P. Wheeler, C. Gu, and Y. Li, "A branch current reallocation based energy balancing strategy for the modular multilevel matrix converter operating around equal frequency," *IEEE Transactions on Power Electronics*, vol. 33, no. 2, pp. 1105–1117, 2018.
- [19] M. Hagiwara and H. Akagi, "Control and Experiment of Pulsewidth-Modulated Modular Multilevel Converters," *IEEE Transactions on Power Electronics*, vol. 24, no. 7, pp. 1737–1746, July 2009.
- [20] A. Antonopoulos, L. Angquist, and H. Nee, "On dynamics and voltage control of the Modular Multilevel Converter," in *2009 13th European Conference on Power Electronics and Applications*, Sep. 2009, pp. 1–10.
- [21] IEEE Standards Association, "IEEE Standard Requirements for Liquid-Immersed Distribution Substation Transformers," *IEEE Std C57.12.36-2017 (Revision of IEEE Std C57.12.36-2007)*, pp. 1–39, Aug 2017.
- [22] M. M. C. Merlin and T. C. Green, "Cell capacitor sizing in multilevel converters: cases of the modular multilevel converter and alternate arm converter," *IET Power Electronics*, vol. 8, no. 3, pp. 350–360, 2015.
- [23] CENELEC, "EN 62751-1:2014 Power losses in voltage sourced converter (VSC) valves for high-voltage direct current (HVDC) systems Part 1: General requirements," BSI, Tech. Rep., 2014.
- [24] CENELEC, "EN 62751-2:2014 Power losses in voltage sourced converter (VSC) valves for high voltage direct current (HVDC) systems Part 2: Modular multilevel converters," BSI, Tech. Rep., 2014.
- [25] P. S. Jones and C. C. Davidson, "Calculation of power losses for MMC-based VSC HVDC stations," in *2013 15th European Conference on Power Electronics and Applications (EPE)*, Sep. 2013, pp. 1–10.
- [26] J. Zang, J. Wang, J. Zhang, and J. Zhou, "Overview of grounding schemes for solid-state transformers in distribution networks," *IET Generation, Transmission & Distribution*, vol. n/a, no. n/a. [Online]. Available: <https://ietresearch.onlinelibrary.wiley.com/doi/abs/10.1049/gtd2.12249>
- [27] "Ieee guide for safety in ac substation grounding," *IEEE Std 80-2013 (Revision of IEEE Std 80-2000/ Incorporates IEEE Std 80-2013/Cor 1-2015)*, pp. 1–226, 2015.



Pablo Bravo (S'14-M'19) was born in Santiago, Chile. He received the B.Sc. degree in electrical engineering and the M.Sc. in electrical engineering in 2021, all from the Pontificia Universidad Católica de Chile, Santiago, Chile. In 2019 he started working as Research and Development Engineer in Reborn Electric Motors (REM), a Chilean engineering B-Corp that builds new electric vehicles, retrofits old buses and develops solutions for green hydrogen transportation. Currently, he works at REM as the Plant Manager of the first electric vehicle factory in

Chile. His research interests include the development of electromobility in Latin America and power electronics applied to electric networks, electric vehicles and renewable energy.



Javier Pereda (S'09–M'14) received the B.Sc. (Eng.) degree with highest honors in electrical engineering in 2009, and the M.Sc. and Ph.D. degrees in electrical engineering in 2013, all from Pontificia Universidad Católica de Chile (PUC), Santiago, Chile. In 2013, he joined the Electrical Department of Pontificia Universidad Católica de Chile, where he is currently Associate Professor. From 2014 to 2016, he was an Associate Research of the Control and Power Group, Department of Electrical and Electronic Engineering, Imperial College London.

He is an Associate Research of the Solar Energy Research Center, Chile, and the UC Energy Research Center, Chile. He is a Principal Investigator of the Electric Vehicle Laboratory and the Power and Energy Conversion Laboratory (PEClab), Pontificia Universidad Católica de Chile. His research interests include power electronics and control applied to electric vehicles, energy storage, ac and dc electric networks and microgrids, renewable energy, multilevel converters, industrial applications, and motor drives.



Felix Rojas (S'09–M'12) was born in Santiago, Chile. He received the B. Eng. and M.Sc. degrees in electrical engineering (Hons.) from the Universidad de Santiago de Chile, Santiago, in 2009, and the doctoral degree in electrical engineering from the Technical University of Munich, Munich, Germany, in 2016. From 2016 to 2021, he was Associate Professor at the Electrical Engineering with the University of Santiago, Chile and head of the Electrical Energy Technologies Research Center (E2TECH) at USACH. Currently, he is Associate Professor at the

Electrical Department with the Pontificia Universidad Católica de Chile and a Principal Investigator of the Electric Vehicle Laboratory and the Power and Energy Conversion Laboratory (PEClab). He is also Associate Research with the Solar Energy Research Center (SERC Chile) and the UC Energy Research Center. His research interests are in control of Modular Multilevel Converters, Solid State Transformers, renewable energy conversion, electric vehicles chargers and machine drives.



Michael M. C. Merlin (M12) received the Electrical Engineering degree from the Ecole National Supérieur de l'Electronique et de ses Applications (ENSEA), Cergy, France, in 2008 and the M.Sc. degree in control systems then the Ph.D. degree in electrical engineering from Imperial College, London, U.K. in 2008 and 2013 respectively. He became a Lecturer at the University of Edinburgh in 2017. His main research interest are design, optimization and control of power converters, more specifically of the modular types which use stacks of sub-modules

to achieve high power efficiency and waveform quality.



Sebastián Neira (S'18) received the B.Sc.(Eng.) degree in electrical engineering from the Pontificia Universidad Católica de Chile, Santiago, Chile, in 2016. He is currently working toward the Ph.D. degree in the dual-degree Ph.D. program between the Pontificia Universidad Católica de Chile and the University of Edinburgh, Edinburgh, U.K. Since 2017, he has been with Power and Energy Conversion Laboratory, Pontificia Universidad Católica de Chile. His current research interests include the design and control of multiport and multilevel power

converters applied to energy storage, solar energy conversion, and industrial applications.



Timothy C. Green (Fellow, IEEE) received the B.Sc. (Eng.) degree (Hons.) from Imperial College London, U.K., in 1986, and the Ph.D. degree from Heriot-Watt University, Edinburgh, U.K., in 1990. He is currently a Professor of Electrical Power Engineering with Imperial College London, and the Co-Director of the Energy Futures Lab with a role of fostering interdisciplinary energy research across the university. His research uses the flexibility of power electronics to enable electricity networks to operate with very high fractions of low carbon technologies.

In HVDC, he has contributed converter designs that strike improved trade-offs between power losses, physical size, and fault handling. In distribution systems, he has pioneered the use of soft open points. He has made important contribution to the study of stability of grid-connected inverters. He is also a Chartered Engineer in the U.K. and a Fellow of the Royal Academy of Engineering.